1. AGENCY USE ONLY (Leave blank)	2. REPORT DATE	3. REPORT TYPE AND DATES COVERED
	31 March 1993	01 April 1990 - 31 March 1993 FINAL

4. TITLE AND SUBTITLE
(U) RECEPTIVITY OF BOUNDARY LAYERS TO CONVECTED GUSTS

5. FUNDING NUMBERS
PE - 61102F
PR - 2307
SA - BS
C - F49620-90-C-0031

6. AUTHOR(S)
D. E. Parekh

7. PERFORMING ORGANIZATION NAME(S) AND ADDRESS(ES)
McDonnell Douglas Aerospace
P. O. Box 516
St. Louis, MO 63166-0516

AFOSR-TR-

8. PERFORMING ORGANIZATION REPORT NUMBER
MDC 93B0041

9. SPONSORING/MONITORING AGENCY NAME(S) AND ADDRESS(ES)
AFOSR/NA
Building 410
Bolling AFB DC 20332-6448

10. SPONSORING/MONITORING AGENCY REPORT NUMBER
F49620-
90-C-0031

11. SUPPLEMENTARY NOTES

12a. DISTRIBUTION/AVAILABILITY STATEMENT
Approved for public release; distribution is unlimited

12b. DISTRIBUTION CODE
Original contains color plates: All DTIC reproductions will be in black and white

13. ABSTRACT (Maximum 200 words)

The primary objective of this study is to determine experimentally the receptivity of a laminar boundary layer to convected gusts. Receptivity is the process by which external disturbances transfer energy to instabilities in the boundary layer. The term convected gust refers to a transient or periodic vortical disturbance convected by the freestream. The experimental approach consisted of hot-wire studies of the boundary layer response to vortical disturbances produced by an array of oscillating ribbons. The boundary layer is remarkably insensitive to large-scale vortical perturbations. No significant Tollmien-Schlichting waves were observed. The vortical disturbances are rapidly damped in the boundary layer and cause only weak oscillations that are primarily of the same frequency and wavelength as the external disturbance.

14. SUBJECT TERMS	15. NUMBER OF PAGES
Receptivity; Boundary Layer Transition; Wakes; Boundary Layer Instabilities	42
	16. PRICE CODE

17. SECURITY CLASSIFICATION OF REPORT	18. SECURITY CLASSIFICATION OF THIS PAGE	19. SECURITY CLASSIFICATION OF ABSTRACT	20. LIMITATION OF ABSTRACT
Unclassified	Unclassified	Unclassified	UL

PREFACE

The work reported here was performed by McDonnell Douglas Aerospace (MDA) in St. Louis, Missouri, for the United States Air Force Office of Scientific Research, Bolling Air Force Base, Washington, DC, under Contract F49620-90-C-0031. The work reported was conducted in the Experimental Fluid Dynamics Group which is a part of the Advanced Flight Technologies program of MDA. The principal investigator is Dr. D. E. Parekh.

The technical report has been reviewed and approved.

Frank W. Spaid

F. W. Spaid
Manager Engineering–Experimental Fluid Dynamics
McDonnell Douglas Aerospace

Rudy Yurkovich

R. N. Yurkovich
Manager Engineering–Advanced Flight Technologies
McDonnell Douglas Aerospace

List of Pages

TABLE OF CONTENTS

LIST OF FIGURES

1. EXECUTIVE SUMMARY

This report describes the results of an experimental study of boundary layer receptivity to convected gusts. Receptivity is the process by which external disturbances, such as sound and freestream turbulence, enter a laminar boundary layer and trigger the transition to turbulent flow. An understanding of the receptivity process is critical to major improvements in the current capability to predict boundary layer transition and to design laminar flow control systems.

The primary objective of this work is to determine experimentally the receptivity of a laminar boundary layer to convected gusts. The term "convected gust" refers to a transient or periodic vortical disturbance convected by the freestream flow. Considerable effort was devoted to characterizing the convected gust so that the boundary layer response to the disturbance could be properly understood.

The experimental approach consisted of studying a laminar boundary layer on a highly polished flat plate in a low-disturbance wind tunnel. Careful measurements were made to assure that background sound, plate vibrations, and freestream turbulence were sufficiently low so that receptivity could be measured. An array of oscillating ribbons produced the convected gust, and a hot-wire probe provided high accuracy resolution of the resulting velocity fluctuations in the boundary layer.

The following observations summarize the key results of this work. First, the boundary layer is remarkably insensitive to large-scale vortical perturbations even in the vicinity of leading edges and surface discontinuities. No significant Tollmien-Schlichting waves were observed. Second, while external vortical disturbances are rapidly damped in the boundary layer, these disturbances can initiate weak oscillations in the boundary layer that have the same frequency and wavelength as the external disturbance. Third, the wake of an array of oscillating ribbons transitions from a simple wavy wake to a discrete vortex street for Strouhal numbers above 0.2, based on ribbon chord length. The transition in wake patterns results in many stable hybrid patterns for Strouhal numbers between 0.2 and 0.3.

2. NOMENCLATURE

A	=	rms amplitude of ribbon acceleration, m/s^2
f	=	frequency, Hz
F	=	non-dimensional frequency, $2\pi fv / U_0^2$
h	=	step height, mm
Re_{0h}	=	step-height Reynolds number, $U_0 h/v$
Re_{δ^*}	=	displacement-thickness Reynolds number, $U_0 \delta^*/v$
U_0	=	average freestream velocity, m/s
u'	=	streamwise velocity component at excitation frequency, m/s
v'	=	normal velocity component at excitation frequency, m/s
v_r	=	normal velocity of ribbons (measured at drive block), m/s
x	=	streamwise distance from leading edge of plate, mm
X_0	=	streamwise distance between gust device and leading edge, mm
y	=	normal distance from wall, mm
Y_0	=	vertical distance between gust device and leading edge, mm

Greek symbols:

δ^*	=	displacement thickness, mm
v	=	kinematic viscosity, m^2/s

3. INTRODUCTION

The transition of a boundary layer from laminar to turbulent flow is a critical factor in a wide variety of applications. Design of laminar flow control systems for viscous drag reduction requires a solid understanding of the transition process. Even in flows that are primarily turbulent, transition can be important. For example, on supercritical wings, where and how transition occurs can significantly impact shock location. This in turn alters both the drag and the pitching moment of the wing.

Boundary layer transition typically involves a series of stages as shown conceptually in Fig. 1. External disturbances, such as freestream turbulence and sound, generate disturbances in the boundary layer which can grow through linear and non-linear mechanisms, resulting in transition to turbulent flow. Receptivity, the first stage, is the process by which external disturbances, such as freestream turbulence and sound, generate Tollmien-Schlichting (T-S) instability waves in a laminar boundary layer. Much research has been devoted in the last 50 years to studying the growth and evolution of disturbances in the laminar boundary layer, but only recently has significant attention been focused on how those disturbances are initiated.

In the case where the wavelength of the external disturbance is much larger than the T-S wavelengths, a wavelength conversion mechanism is needed to transfer energy from the disturbance to T-S waves in the boundary layer. Using high Reynolds number asymptotic methods, Goldstein (1983, 1985) showed that this wavelength conversion occurs where the mean boundary layer flow experiences rapid changes in the streamwise direction, for example, in the leading edge region or near a surface bump. Nishioka and Morkovin (1986) showed that gradients in the forcing field could also cause the formation of T-S waves.

Reviewing recent progress in the theoretical understanding of receptivity phenomena, Kerschen (1990) compares receptivity to convected gusts and to plane acoustic waves at a leading edge and at a surface bump. For both acoustic and convected gust receptivity at the leading edge, the receptivity coefficient increases with disturbance incidence angle to a local maximum at an angle of 90 degrees for the convected gust and of 180 degrees for the plane

acoustic wave. The receptivity coefficient is much less than unity for both types of disturbances when the incidence angle is 0 degrees. For an acoustic wave, 0-degree incidence angle corresponds to an acoustic wave propagating downstream parallel to the wall; for a convected gust, this angle corresponds to a vortical disturbance whose wave vector is parallel to the wall. At a surface bump, receptivity to an acoustic disturbance is much greater than receptivity to a convected gust because the boundary layer is more sensitive to forcing close to the wall (acoustic mechanism) than to forcing at its outer edge (convected gust mechanism). With asymptotic methods, Kerschen (1991) also analyzed the case of a vortex street propagating outside of the boundary layer.

There have been relatively few experimental or computational efforts that have focused on receptivity to vortical disturbances. Kachanov *et al.* (1978) considered the effect of a vortex street propagating close to the boundary layer so as not to impinge directly on the 25:1 elliptic leading edge (50-mm long) but to approach the edge of the growing boundary layer downstream of the leading edge. A single oscillating ribbon (0.1-mm thick by 3-mm wide by 180-mm long) upstream of the leading edge produced the vortical disturbance. They found that the amplitude of the disturbance decays rapidly in the boundary layer and found no evidence of T-S waves downstream of the leading edge. T-S waves, observed only on the leading edge, decayed rapidly to 1/8th of their peak amplitude within the first 15 mm. Thus, they conclude that no appreciable generation of T-S waves occurs (see also Dovgal *et al.*, 1979).

In a recent Navier-Stokes simulation of receptivity to a vortical disturbance at a 6:1 elliptic leading edge, however, Buter and Reed (1993) found clear evidence of T-S response. The T-S response varied linearly with forcing amplitude whether the disturbance was symmetric or asymmetric relative to the leading edge. They also found evidence of a decaying superharmonic component as a result of asymmetric forcing.

Instead of looking at a single frequency vortical disturbance, Kendall (1991) considered broadband vortical disturbances generated by an array of small jets located upstream of the

wind tunnel contraction. His surface measurements of fluctuating pressure indicated that T-S waves are not only generated at the leading edge but are also continually excited in the streamwise direction. This resulted in T-S waves that grow faster than predicted by linear theory. Thus, he explains his findings in terms of localized receptivity at the leading edge and of distributed receptivity involving the continuous transfer of energy to the boundary layer along the surface length.

In this work we consider boundary layer receptivity to convected single frequency vortical disturbances, which represent components of freestream turbulence. Specifically, we consider receptivity to a spatially periodic convected gust at a leading edge and at surface discontinuities. This report presents a description of the gust-generating device, a characterization of the convected gust, and a discussion of the receptivity results. The concluding remarks also include some possible explanations for the apparent discrepancies among the different studies referenced above.

This research is one part of a collaborative effort in receptivity sponsored by the Air Force Office of Scientific Research. The total effort also includes separately funded analytical, experimental, and computational research by Dr. E. J. Kerschen at the University of Arizona and Drs. W. S. Saric and H. L. Reed at Arizona State University. This multi-faceted approach provides an effective means for dealing with the complexity of the receptivity process.

4. OBJECTIVES

The general objective of this work is to determine experimentally the receptivity of a laminar boundary layer to convected vortical disturbances. Specific objectives for this effort include the following:

1) Determine a suitable device for the generation of a convected vortical disturbance and document the characteristics of that disturbance,

2) Investigate the effect of leading edge bluntness and surface discontinuities on boundary layer receptivity to vortical disturbances, and

3) Compare results with other investigations, in general, and with the theoretical results of Kerschen, in particular.

5. APPROACH

The experimental approach consisted of studying a laminar boundary layer on a highly polished flat plate in a low-disturbance wind tunnel. Careful measurements were made to assure that background sound, tunnel vibrations, and freestream turbulence are sufficiently low so that receptivity can be measured. An array of oscillating ribbons produced the convected gust, and a hot-wire probe measured the resulting velocity fluctuations in the boundary layer. Real-time calculations of the frequency spectra of the velocity fluctuations provided a high accuracy measurement of the frequency components of interest. The remainder of this section describes this experimental approach in more detail. Figure 2 presents a schematic of the experimental apparatus.

Experimental Apparatus

The facility used in this work is a closed-return, blower-driven wind tunnel. The test section of this tunnel measures 0.91-m wide by 0.66-m high by 5.5-m long, and its inlet contraction has a 9:1 area ratio. Streamwise velocity fluctuations, measured by a hot-wire anemometer with a low-pass filter at 10 kHz, are typically 0.1% or less of the freestream mean velocity. Even with a forward-facing step on the boundary layer plate (see Fig. 2), transition could not be obtained at Reynolds numbers up to 2.6 million. Traverse position and tunnel speed limits made higher Reynolds numbers unobtainable.

The boundary layer plate was fabricated from polished, 13-mm-thick aluminum tooling plate for the convected gust receptivity work. The 2.9-m-long plate was mounted from the sides in the vertical center of the tunnel on vibration-damping rails. A set of interchangeable 6:1, 12:1, and 24:1 (ratio of major to minor radii) elliptic leading edges were made by

machining one end each of three identical 508-mm-long flat plates. This approach provides a smooth transition from the elliptic profile to the flat section, avoiding the surface discontinuity that results when the elliptic section is machined as a separate part.

The plate junction at x = 508 mm could be adjusted by means of locating pins to produce a desired surface discontinuity. For some cases, the junction had a 0.11-mm forward-facing step (+/- 0.02 mm over the center section and +/- 0.04 mm over the entire span). In the rest of the cases, a strip of precision stainless steel thickness gauge stock was cemented at the junction as shown in Fig. 2 to provide a rectangular bump (0.18 mm by 12.7 mm, including adhesive). The plate was oriented at a very slight angle of attack (< 0.5°) to achieve a nominal zero-pressure-gradient boundary layer (shape factor of 2.59 +/- 0.04) over the x-range of 350 to 1050 mm. The trailing-edge flap was set between 5 and 7 degrees to position the stagnation line slightly on the test side of the plate.

Unlike sound, which one can easily produce with a loudspeaker, a convected gust is more difficult to generate. Since an arbitrary gust could be decomposed into a set of single-frequency gusts of varying orientations, it is desirable to be able to control the wave number and orientation of the convected gust. This rules out any type of steady wake. One could generate a gust by traversing a bluff body, such as a cylinder, across the flow upstream of the leading edge or by pulsing a jet. However, the advantages of a periodic disturbance, practical implementation considerations, and the desirability of a single-wave-number gust of variable orientation motivated a different approach: an array of oscillating ribbons.

An array of ribbons, positioned 400 mm upstream of the leading edge, provided the convected gust excitation (see Figs. 2 and 3). The vertical position of the array could be continuously varied from near the bottom wall up to the center of the tunnel. The vertical distance between the tip of the leading edge and the center of the ribbon array is denoted by Y_0. The relative streamwise position of the ribbons can be adjusted to produce periodic gusts of various inclinations, β. When all the ribbons are aligned vertically, a 0-degree inclination of the vortical disturbance is produced. The number of ribbons, N, were varied

from 1 to 10. Choosing a large number of ribbons allows one to create a disturbance whose vertical extent is on the order of its streamwise wavelength. Such a large (in size) disturbance was deemed necessary to compare with some of the analytical results of Kerschen.

A pair of electro-magnetic shakers drove the ribbons in phase, and accelerometers mounted on each driving block measured the excitation level. The fundamental resonance frequency, which was set by adjusting the ribbon tension, typically ranged from 90 to 110 Hz. By using excitation frequencies below this fundamental resonance, we avoided the excitation of higher order modes on the ribbon. Measurements of ribbon displacement indicated that the amplitude in the center of the ribbons was typically 1.5 to 2 times that at the driving blocks, depending on frequency. The center displacement can be predicted fairly well by a single spring-mass system model. The tension in the ribbons was sufficient to avoid aerodynamically induced oscillations at flow velocities up to 10 m/s; the receptivity experiments described here considered only velocities below 10 m/s.

Data Acquisition and Analysis

Velocity was measured by a single hot-wire sensor mounted on an automated traversing system utilizing micro-stepper motors and a precision linear position indicator. Traverse control and all data acquisition were performed on a VAXlab data-acquisition and processing system. The hot-wire signal was directly digitized and linearized using a fourth-order polynomial and temperature compensation. The hot-wire signal was also band-pass filtered about the excitation frequency, amplified, digitized on a second channel, and linearized based on the mean-flow measurement. This technique provided high-precision measurements of the disturbance velocity component. An x-wire probe provided detailed measurements of the wake behind the oscillating ribbon array.

A multi-channel FFT algorithm was used to provide high-accuracy, narrow-band phase and amplitude measurements in real time. The spectrum of the hot-wire signal was computed to obtain the narrow-band amplitude at the excitation frequency. Computation of the

complex cross-spectrum provided phase and coherence relative to the reference excitation signal.

Flow visualization provided clear images of the wake patterns behind the array of oscillating ribbons. A compact stream of smoke introduced upstream of the inlet contraction was illuminated by a light sheet from an argon-ion laser. Pictures were taken with a 35-mm camera on TMAX 3200 or EKTAR 1000 film at fast shutter speeds (1/2000 to 1/8000 sec.) to freeze the motion of the wake.

6. CHARACTERIZATION OF DISTURBANCE

In this and the next sections, we consider both the characteristics of the convected gust and the boundary layer response to this convective disturbance. In the experiments conducted to date, receptivity was investigated over a range of freestream velocities (6 to 10 m/s), ribbon excitation frequencies (50 to 70 Hz) and amplitudes (2.0 to 49.0 m/s^2), gust device placement ($-63.5 \le Y_0 \le 0$ mm), and number of ribbons ($1 \le N \le .\ 10$) A subset of those results are discussed here.

Wake Patterns

The individual wakes of the ribbons merge to produce a combined wake well ahead of the boundary layer plate location. With no excitation, the flow behind the ribbons appears undisturbed. With excitation, the general shape of the combined wake changes from a sine wave to a discrete vortex street as the Strouhal number ($St = fL/U$) is increased (Fig. 4). The transition from a wavy wake to a discrete vortex street occurs over the range $0.2 < St < 0.3$. Within this range the wake exhibits a hybrid pattern of discrete vortices superimposed on a wavy wake. Increasing the number of ribbons, N, or varying the array inclination angle, β, increases the complexity of the wake patterns even further (Fig. 5).

Disturbance Velocity Field

To characterize the disturbance produced by the combined wake, a set of velocity profiles spaced 20 mm apart in the streamwise direction were measured without the plate. The mean

wake profile has a symmetric velocity deficit which in the far field decays with x (Fig. 6). However, the velocity deficit has a local peak at $x-x_0 = 30$ mm for $U_0 = 7$ m/s and at $x-x_0 = 200$ mm for $U_0 = 9$ m/s. The fact that the downstream shift of the peak is proportional to the mean velocity ($x = 430$ mm for $U_0 = 7$ m/s and $x = 600$ mm for $U_0 = 9$ m/s) indicates that the peak location scales with the wavelength of the wavy wake. This, along with visualization images, suggests that this local peak of the mean velocity deficit might be caused by the saturation of the growth of the wake instability. These cases correspond to a high excitation level ($A = 49$ m/s^2) used typically when the wake is positioned away from the plate; in cases for which the wake is aligned with the plate, the excitation amplitudes used are typically lower ($A = 9.8$ m/s^2).

The amplitude and phase profiles of the fundamental component of the streamwise (Fig. 7) and normal (Fig. 8) perturbation velocities provide important documentation of the disturbance field for the N=10 case. The amplitudes of the fundamental components of both the streamwise and normal velocity fluctuations, u' and v', remain relatively constant with x up to the end of the measurement domain, 1 m downstream from the ribbons. The variation in y, however, is not identical. The u' component has peaks at the edge of the wake and a 180-degree phase shift across the wake. The v' component is constant in amplitude within the core of the wake and is essentially uniform in phase across the wake at any given streamwise position. These characteristics are consistent with the wake structure observed by flow visualization.

Profiles of the streamwise perturbation velocity amplitude and phase for the single ribbon case are given in Fig. 9. These measurements were made with a single-wire probe and with the plate installed. With symmetric excitation, the shakers drove the ribbons in phase at identical frequency and amplitude. The asymmetric excitation was achieved by reducing the amplitude of one shaker by a factor of 10 relative to the other shaker. The asymmetric excitation resulted in a weaker and narrower perturbation field at the mid-span location as one would expect. The apparent absence of a double-peak amplitude profile in two of the

three cases could simply be a result of the coarse spatial resolution of these profiles. The phase profiles exhibit the same 180° phase shift across the wake (Fig. 9b) as seen for the multiple ribbon wake (Fig. 7b).

7. BOUNDARY LAYER RESPONSE

The previous section characterized the vortical disturbance through flow visualization and single-wire and x-wire measurements. In this section, we discuss measurements of the boundary layer response to the external vortical disturbance. Since the boundary layer is very thin (on the order of 1 mm), only a single-wire probe is used in the boundary layer.

The mean boundary layer velocity profiles for a variety of cases collapse onto the theoretical Blausius profile of a zero-pressure-gradient boundary layer (Fig. 10). Slight deviations from the theoretical profile are observed only when the gust excitation is present. When the wake impinges on the plate ($Y_0 = 0$), the mean boundary layer profile remains the same as in the no wake case over the range of $250 \leq x \leq 650$ with shape factor equal to 2.59 +/- 0.04. Outside this range, the shape factor decreases to about 2.45 at $x = 1050$ for excitation at $A = 9.81$ m/s^2 and $f = 50$ or 70 Hz. Lower shape factors are also measured for single-ribbon excitation at $Y_0 \gg 0$. These lower shape factors correspond to a slightly favorable pressure gradient, which has the effect of stabilizing the flow by reducing the size of the streamwise region over which disturbances grow.

To distinguish leading edge receptivity from receptivity at the step, measurements are made upstream and downstream of the surface discontinuity. Figures 11-13 correspond to the case of a multiple ribbon (N=10; β=0°) wake impinging symmetrically ($Y_0 = 0$) on the leading edge. To provide a local receptivity site, the plates are misaligned slightly to produce a 0.11-mm forward-facing step at $x = 508$ mm. Clusters of y-profiles of the velocity component at the frequency of excitation are shown in Fig. 11. All the profiles in each cluster essentially collapse on each other indicating that the convected gust disturbance is the only significant component of the measured velocity field. Some of the scatter that exists is

due to the uncertainty in the normalizing parameter, δ^*, which is computed independently at each x location.

In all the velocity profiles shown in Fig. 11, there is a peak at the edge of the boundary layer at $y/\delta^* = 3$. The other peak in the freestream corresponds to the peak in the u' disturbance produced at the edges of the gust device. The location of the inner peak scales with the boundary layer thickness while the location of the outer peak appears to scale with the width of the convected gust. As the boundary layer grows with x, the two peaks merge. Once the peaks have merged (Fig. 11d), the shape of the velocity profile is similar to that of a typical T-S mode.

The phase profiles corresponding to the amplitude profiles in Fig. 11 are shown in Fig. 12. Outside the boundary layer, there is a consistent phase variation with x corresponding to the wavelength ($\approx$ 150 mm) and phase speed ($\approx 0.94\ U_0$) of the disturbance. For the most upstream profiles (Figs. 12a and 12b), there is a phase shift with y of about 100 degrees outside the boundary layer. This results from the fact that the convected gust, whose u' component has a 180-degree phase shift across the gust, is split in half by the plate. Within the boundary layer the phase varies linearly a full 360 degrees as one moves toward the wall. The phase profile at x = 1050 mm (Fig. 12d) has a 180 degree phase shift at the y-location corresponding to the local minimum of its corresponding amplitude profile (Fig. 12d); this too is a remarkable similarity to T-S wave characteristics.

A set of velocity profiles extending further in y are shown in Fig. 13 for a range of x locations and two different excitation frequencies, $F=81 \times 10^{-6}$ (Fig. 13a) and $F=113 \times 10^{-6}$ (Fig. 13b), where $F \equiv 2\pi f\nu/U^2_0$. For both cases, the step location ($Re_{\delta^*} = 824$) corresponds to a point within the neutral stability curve, and the Reynolds number, R_{0h}, based on freestream velocity and step height is 53. The velocity decays rapidly from the edge of the boundary layer to the wall in all profiles as observed by Kachanov *et al.* (1978). This is very different from the acoustic disturbance (or Stokes layer) for which the amplitude of the disturbance remains high throughout most of the boundary layer. For each excitation case in Fig. 13, the

profiles collapse within the boundary layer. Even though some of the velocity profiles resemble the mode shapes of T-S waves, this does not indicate T-S response in the boundary layer since those profiles do not scale as T-S modes. For example, the local minimum in those velocity profiles is outside the boundary layer instead of being located near $y / \delta^* = 2$.

To investigate the boundary layer response to a wake disturbance that grazes the edge of the boundary layer, we made measurements with the ribbon array moved away from the plate ($Y_0 = 64$ mm, $N = 10$). In this case the peaks in the streamwise disturbance field both lie above the plate. The closest peak is located approximately 10 mm from the plate in the vicinity of the step.

Figures 14 and 15 present disturbance velocity amplitude and phase profiles for this case of the grazing wake disturbance. The disturbance amplitude has a peak just outside the boundary layer and decays rapidly in the boundary layer (Fig. 14a). However, unlike the case of the impinging wake ($Y_0 = 0$), the amplitude does not continue to decrease in the near-wall region ($y / \delta^* < 1$) (Fig. 14b). Upstream of the step ($x = 450$ mm), the near-wall amplitude is constant in y; downstream of the step ($x > 508$ mm), the near-wall amplitude exhibits a single peak in y which grows and decays with x. The streamwise variations in phase (Fig. 15) are generally consistent with the wavelength of the wavy wake. Upstream of the step the phase changes monotonically a full 360° in the boundary layer just as in the impinging wake case. Downstream, however, the phase change is neither monotonic nor a full 360°.

A cluster of measurements in the region $545 \leq x \leq 555$ (Fig. 16) shows no variation in amplitude with x and only a slight variation of phase. Since this distance corresponds to approximately one-quarter of a T-S wavelength, a much larger phase variation would be seen if a T-S wave was the dominant part of the total near-wall disturbance. More likely, the disturbance field is a complex sum of a weak Stokes wave, generated by sound from the oscillating ribbons, and the evolving vortical disturbance. The oscillatory growth in x

(Fig. 14b) of the total near-wall disturbance amplitude might be caused by interference between the Stokes wave and the vortical disturbance.

Kerschen's asymptotic analysis (1991) indentifies two receptivity mechanisms associated with a vortical disturbance interacting with a surface bump. The first mechanism is linear and involves an inviscid interaction outside the boundary layer between the vortical disturbance and the small-scale mean flow gradient due to the bump. The results described above (Figs. 11-16) pertain to that mechanism. The second type of mechanism involves an "acoustic" interaction deep in the boundary layer resulting from the pressure fluctuations produced by the vortical disturbance. Although this second mechanism is a second order effect, its potential importance arises from the fact that the boundary layer is much more susceptible to disturbances near the wall than those outside the boundary layer. An example of this interaction is a vortex street convecting far enough above the surface that its velocity fluctuations at the boundary layer are very weak.

To consider this second mechanism, we positioned a single ribbon at $Y_0 = 102$ mm. This distance was chosen to equal one wavelength of the vortical disturbance with $f = 84$ Hz and $U_0 = 9$ m/s. Configurations included both 6:1 and 12:1 leading edges with a 0.18-mm rectangular bump at $x = 508$ mm (see Fig. 2). The ribbon was oscillated symmetrically and asymmetrically. Asymmetric excitation consisted of driving one shaker at 1/10th the amplitude of the other shaker, producing a spanwise amplitude variation along the ribbon.

Figures 17a and 17b present the streamwise evolution of the disturbance amplitude and phase within the boundary layer for these various cases. As an indication of the probe location within the boundary layer, Fig. 17c provides the corresponding local mean velocity. Near the leading edge, the case with asymmetric excitation shows the greatest response. In all cases there is a sharp decline in amplitude immediately downstream of the bump followed by amplitude growth further downstream. The asymmetric case exhibits a 180° phase jump where the disturbance begins to grow ($x = 690$ mm). Amplitude and phase profiles at different x-stations are given for the asymmetric excitation case in Fig. 18.

Since these measured fluctuations are so small (10^{-5} U_0), the fluctuations might include a significant component due to weak probe vibrations. Even probe vibrations normal to the flow could produce an apparent streamwise fluctuation as a result of the velocity gradient in the boundary layer. Assuming that the probe vibration amplitude is constant, the resulting apparent velocity fluctuation would be proportional to the velocity gradient, du/dy, in the boundary layer. However, the variations in streamwise evolution seen in Fig. 17 for the same excitation conditions and the varying shapes of the disturbance profiles (Fig. 18) cannot be explained by probe vibrations alone. The velocity perturbations shown in Figs. 17 and 18 are probably a combination of contributions from sound, some type of vortical wave, and, possibly, probe vibrations.

For this case of a vortex street "far" from the boundary layer, Kerschen's analysis indicates a strong dependence of receptivity on convection speed, with a minimum in receptivity at a convection speed of 0.94 U_0. Thus, it is not surprising that no conclusive evidence of T-S waves were found. Since the convection speed of these wakes, and wakes in general (Corke 1991), is about 0.94 U_0 regardless of excitation or flow parameters, we could not verify the theoretical dependence on convection speed with this experiment.

8. CONCLUDING REMARKS

In this work, we considered the receptivity of a laminar boundary layer to a vortical disturbance having the form of a wavy wake with a single dominant frequency. It is quite remarkable that, whether the disturbance impinged directly on the leading edge, grazed the edge of the boundary layer, or convected outside the boundary layer, no significant generation of T-S waves were observed. While it seems counterintuitive that such large disturbances do not initiate T-S waves, this result is consistent with other research. Similar findings were reported by Kachanov *et al.* (1978) who studied experimentally the receptivity to a more compact vortical disturbance from a single oscillating ribbon grazing the edge of the boundary layer. The case of the wake impinging on the leading edge is similar to the

case, analyzed by Kerschen (1990), of a 2-D vortical gust at 0° incidence. His analysis indicated minimal receptivity to disturbances at 0° incidence. Negligible receptivity at surface discontinuities to a vortical disturbance "far" from the surface is also consistent with Kerschen's analysis (1991). His analysis predicts negligible receptivity to disturbances propagating at 0.94 times the freestream velocity; that value is the convection speed of far-field wakes in general.

At first glance, these results seem to conflict with the computations of Buter and Reed (1993) and the observations of Kendall (1991). However, there are key differences in the physical scale and impingement characteristics of the vortical disturbances and in leading edge bluntness that could account for the differences. In the work reported here, the vertical extent of the wakes are much larger than the half-thickness (or minor radius) of the leading edge, and the peaks of the streamwise perturbations do not impact directly on the tip of the leading edge. In contrast, the disturbance used by Buter and Reed has a vertical extent smaller than the half-thickness and impinges directly on the leading edge. Thus, for the same peak perturbation amplitude, their disturbance would have a much higher spatial gradient and have a physical scale in the vertical direction on the order of a T-S wavelength. In the work by Kachanov *et al.* (1978), the vertical size of the disturbance was on the order of the plate half-thickness, but the disturbance did not impinge directly on the leading edge. Additionally, the leading edge of Buter and Reed (1993) was much more blunt and, consequently, more "receptive" than that used by Kachanov *et al.* (1978) or that used in this work for the impinging wake cases.

In contrast to these single frequency vortical disturbances, Kendall generated free stream turbulence over a broad spectrum. His vortical disturbance contained many small scale components of various orientations and impinged directly on the leading edge. Kendall also suggested that the vortical disturbance continued to transfer energy to the boundary layer along its length and not just at the leading edge. Thus, the boundary layer is apparently directly receptive to that type of disturbance without any surface small-scale inhomogeneity.

This works also documents the non-T-S boundary layer oscillations induced in the boundary layer by the external perturbation. These oscillations seem to be primarily a combination of vortical waves of the same frequency and wavelength as the external perturbation and of Stokes waves. While the total response may also contain a T-S component, it is too weak to detect.

9. ACKNOWLEDGEMENTS

The gust-generating hardware was developed under a related McDonnell Douglas IRAD program in collaboration with Philippe Pulvin of the Swiss Federal Institute of Technology--Lausanne. The author also thanks Richard Wlezien, Edward Kerschen, William Saric, Jerry Kegelman, Mark Morkovin, Helen Reed, Joseph Kroutil, and Alan Cain for many helpful comments and discussions.

10. REFERENCES

Buter, T. A., and Reed, H. L., 1993, "Numerical Investigation of Receptivity to Freestream Vorticity," AIAA paper 93-0073.

Corke, T. C., 1991, private communication.

Dovgal, A. V., Kachanov, Yu. S., Kozlov, V. V., Levchenko, V. Ya., and Maksimov, V. P., 1979, "Development of Perturbations in the Boundary Layer," Institute of Theoretical and Applied Mechanics, Siberian Section, USSR Academy of Sciences, Novosibirsk, 1979, pp. 4-22, translation available as NASA TM-77986.

Goldstein, M. E., 1983, "Scattering of Acoustic Waves into Tollmien-Schlichting Waves Near a Leading Edge," *J. Fluid Mech.*, Vol. 127, pp. 59-81.

Goldstein, M. E., 1985, "Scattering of Acoustic Waves into Tollmein-Schlichting Waves by Small Streamwise Variations in Surface Geometry," *J. Fluid Mech.*, Vol. 154, pp. 509-529.

Kendall, J. M., 1991, "Studies on Laminar Boundary-Layer Receptivity to Freestream Turbulence near a Leading Edge," in *Boundary Layer Stability and Transition to Turbulence*, ASME FED-Vol. 114, pp. 23-30.

Kerschen, E. J., 1991, "Receptivity of Boundary Layers to Convected Disturbances," in *Boundary Layer Stability and Transition to Turbulence*, ASME FED-Vol. 114, pp. 43-48.

Kerschen, E. J., 1990, "Boundary Layer Receptivity Theory," Appl. Mech. Rev., Vol. 43, pp. S152-S157.

Nishioka, M., and Morkovin, M. V., 1986, "Boundary-Layer Receptivity to Unsteady Pressure Gradients: Experiments and Overview," *J. Fluid Mech.*, Vol. 171, pp. 219-261.

Saric, W. S., Hoos, J. A., and Radeztsky, R. H., 1991, "Boundary-Layer Receptivity of Sound with Roughness" Contract Report CEAS-CR-R-90191, Arizona State University, Tempe, AZ.

10. PUBLICATIONS

The following presentations/papers originated from the present contract:

1. Parekh, D. E., "Experiments on Boundary Layer Receptivity to Convective Disturbances," presented at the Turbulence Structure and Control Conference, Columbus, Ohio, 1-3 April 1991.

2. Parekh, D. E, Pulvin, P., and Wlezien, R. W., "Boundary Layer Receptivity to Convected Gusts and Sound," in *Boundary Layer Stability and Transition to Turbulence*, ASME FED-Vol. 114, pp. 69-75.

3. Parekh, D. E. "Boundary Layer Receptivity to Vortical Freestream Disturbances," manuscript in preparation for submission to *J. Fluid Mechanics*.

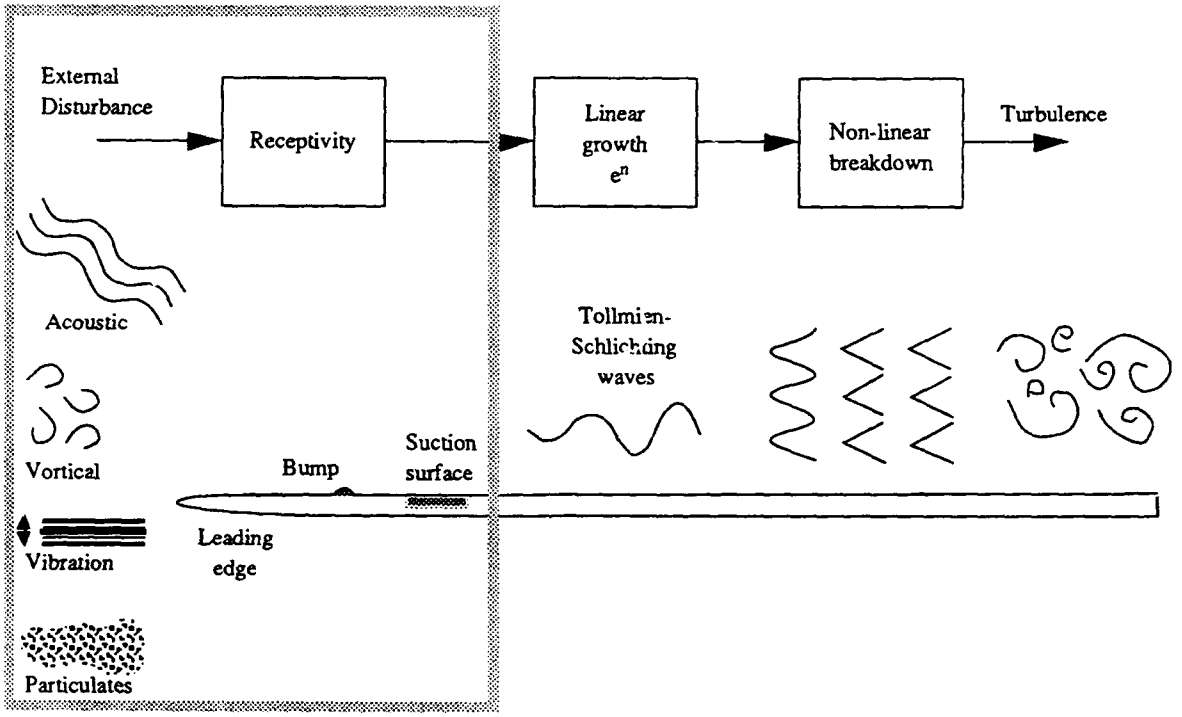

Figure 1. Conceptual diagram of boundary layer transition process.

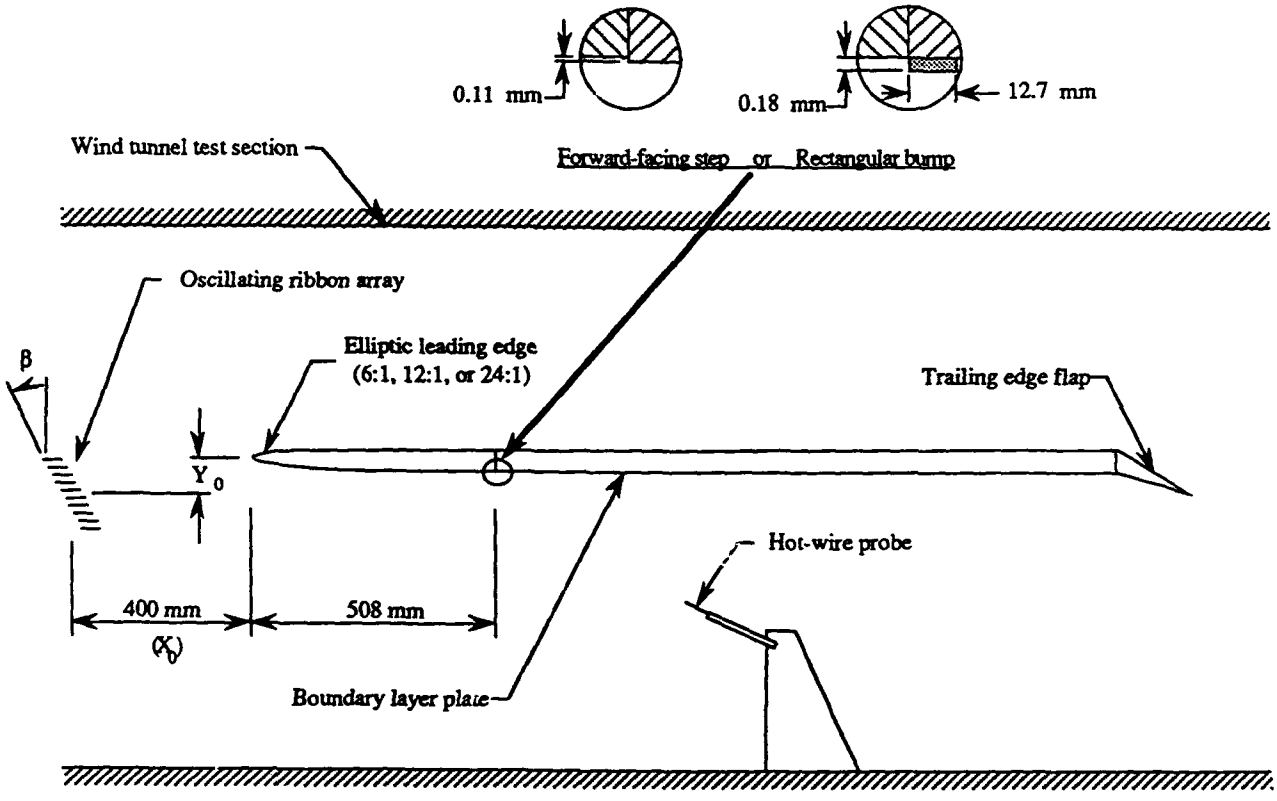

Figure 2. Schematic of experimental appratus.

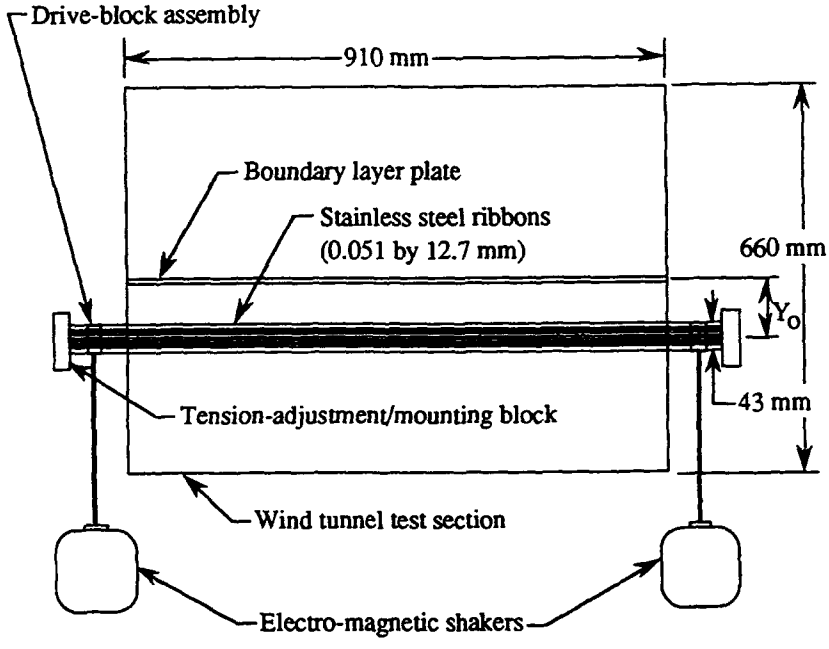

Figure 3. Front view of ribbon assembly and test section.

(a)

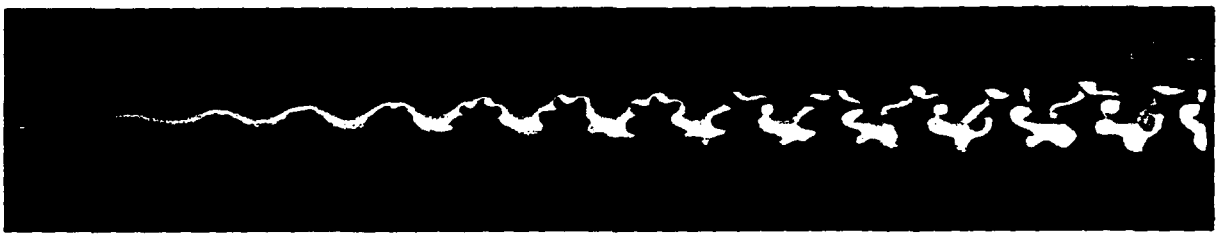

(b)

(c)

Figure 4. Effect of Strouhal number on wake patterns of oscillating ribbons;
(a) St = 0.18, Re = 4060, A = 0.012, U = 5.0 m/s, N = 5, $\beta = 0°$;
(b) St = 0.22, Re = 4080, A = 0.008, U = 5.0 m/s, N = 1;
(c) St = 0.35, Re = 2500, A = 0.008, U = 3.1 m/s, N = 1.

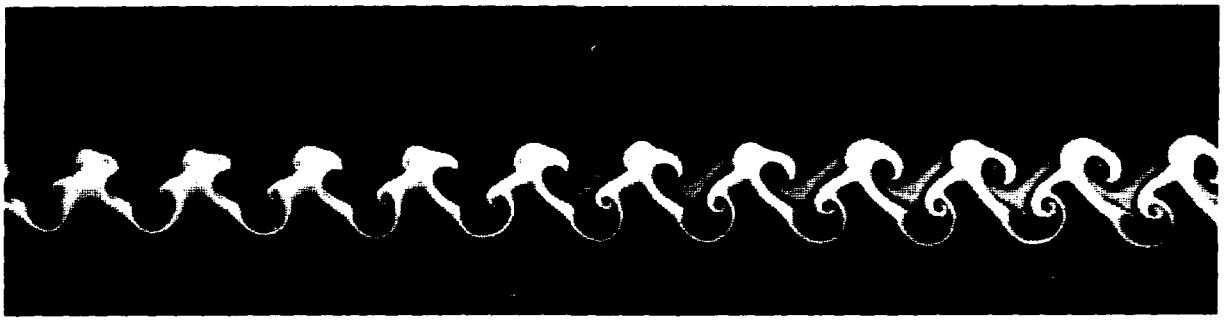

(a)

(b)

(c)

Figure 5. Effect of number and orientation of ribbons on wake patterns;
(a) N = 1, St = 0.27, Re = 3210, A = 0.013, U = 4.0 m/s;
(b) N = 10, $\beta = 0°$, St = 0.29, Re = 2500, A = 0.0093, U = 3.1 m/s;
(c) N = 5, $\beta = 60°$, St = 0.28, Re = 2500, A = 0.0093, U = 3.1 m/s.

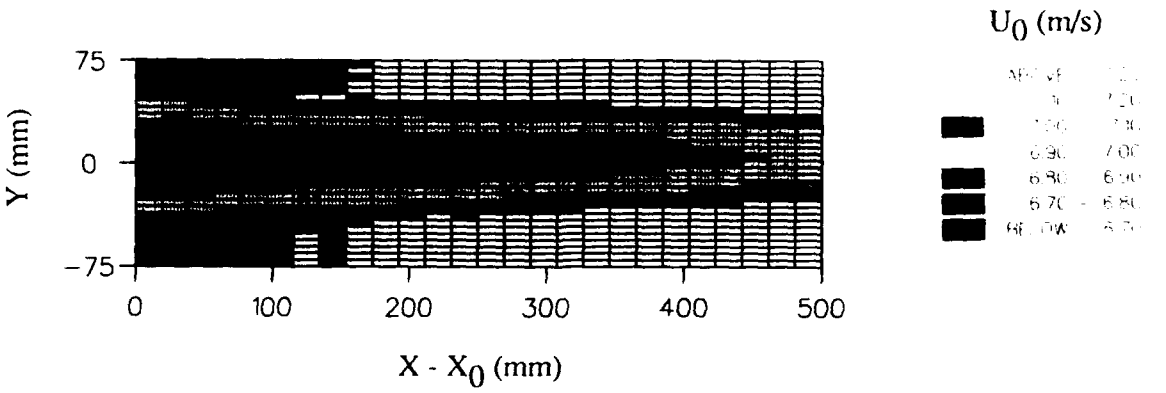

(a)

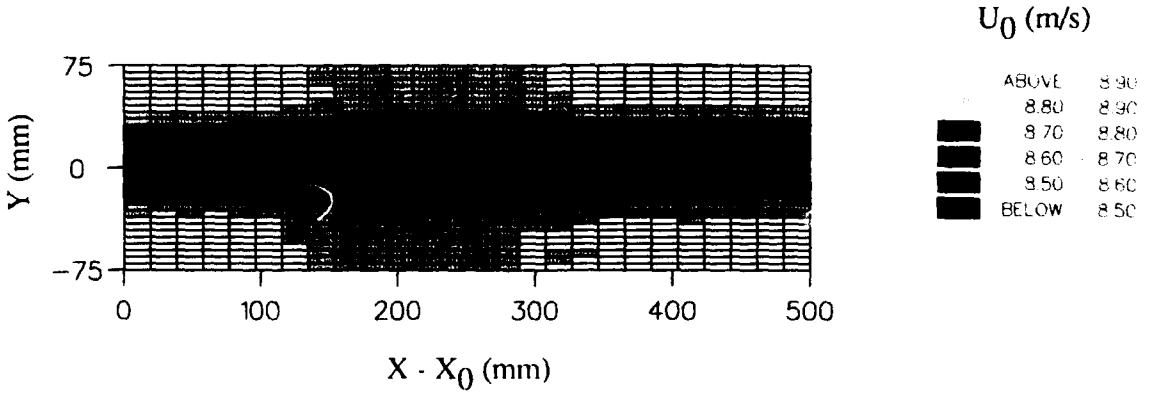

(b)

Figure 6. Mean streamwise velocity field of wake from oscillating ribbons for (a) U_0=7 m/s and (b) U_0=9 m/s. Note that X_0=400 mm and that X is measured from center of ribbon array.

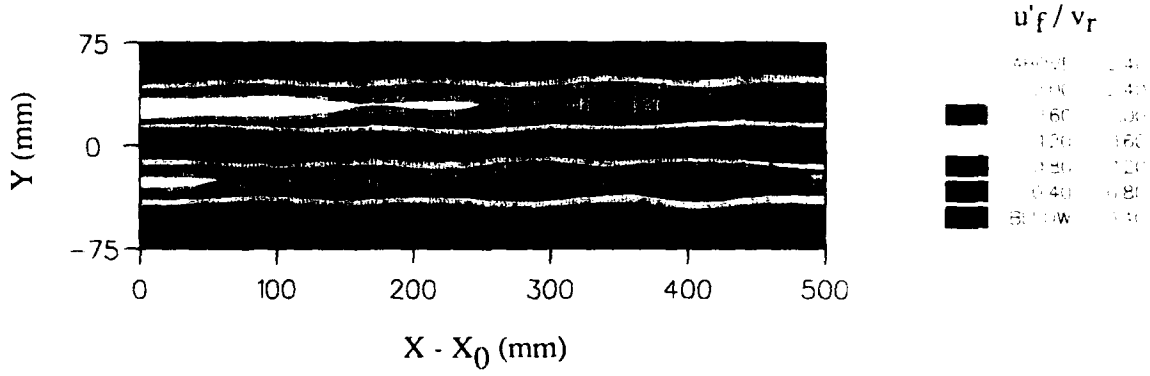

(a)

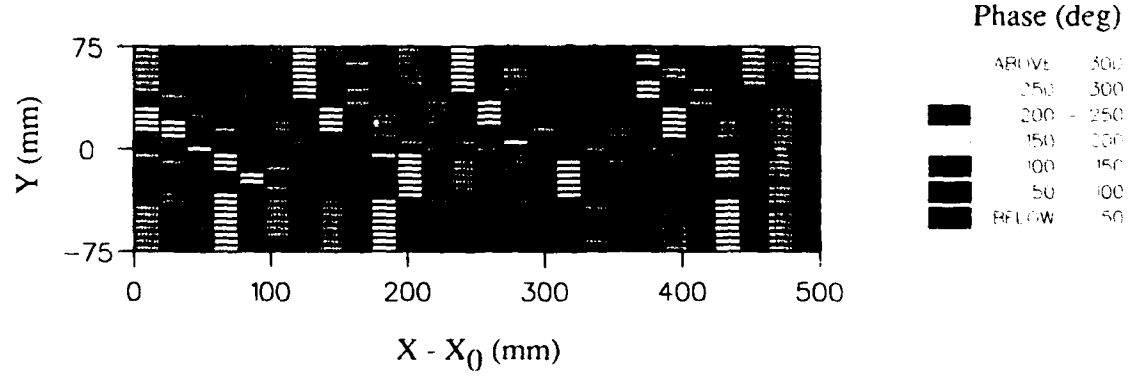

(b)

Figure 7. Profiles of (a) amplitude and (b) phase of fundamental component of streamwise perturbation velocity for $U_0 = 9$ m/s, f = 70 Hz, A = 49 m/s^2, and $v_r = 0.11$ m/s.

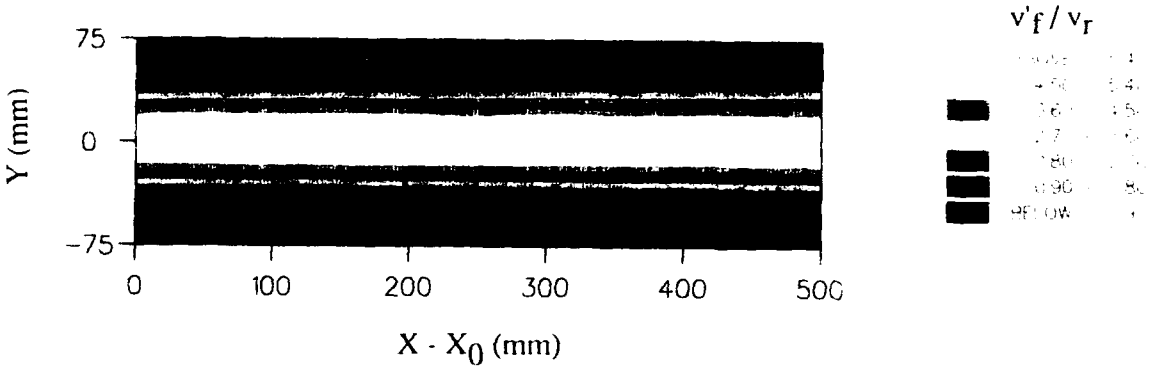

(a)

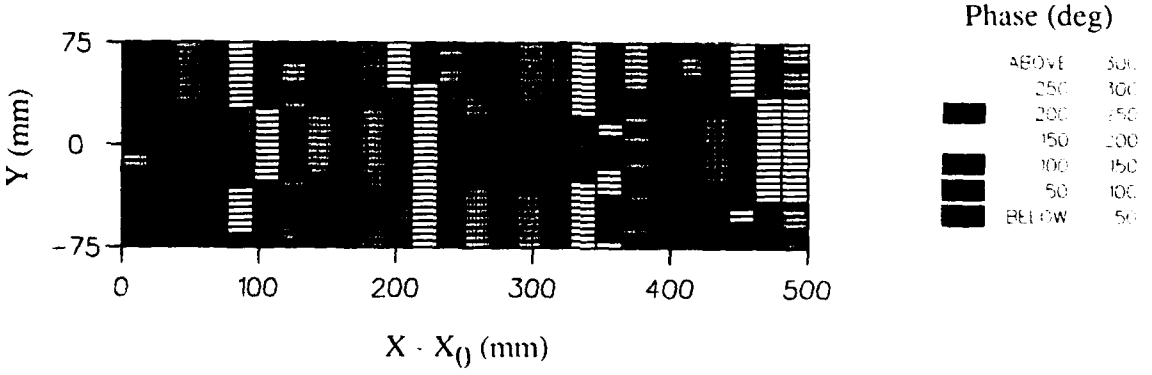

(b)

Figure 8. Profiles of (a) amplitude and (b) phase of fundamental component of normal perturbation velocity for U_0 = 9 m/s, f = 70 Hz, A = 49 m/s^2, and v_r = 0.11 m/s.

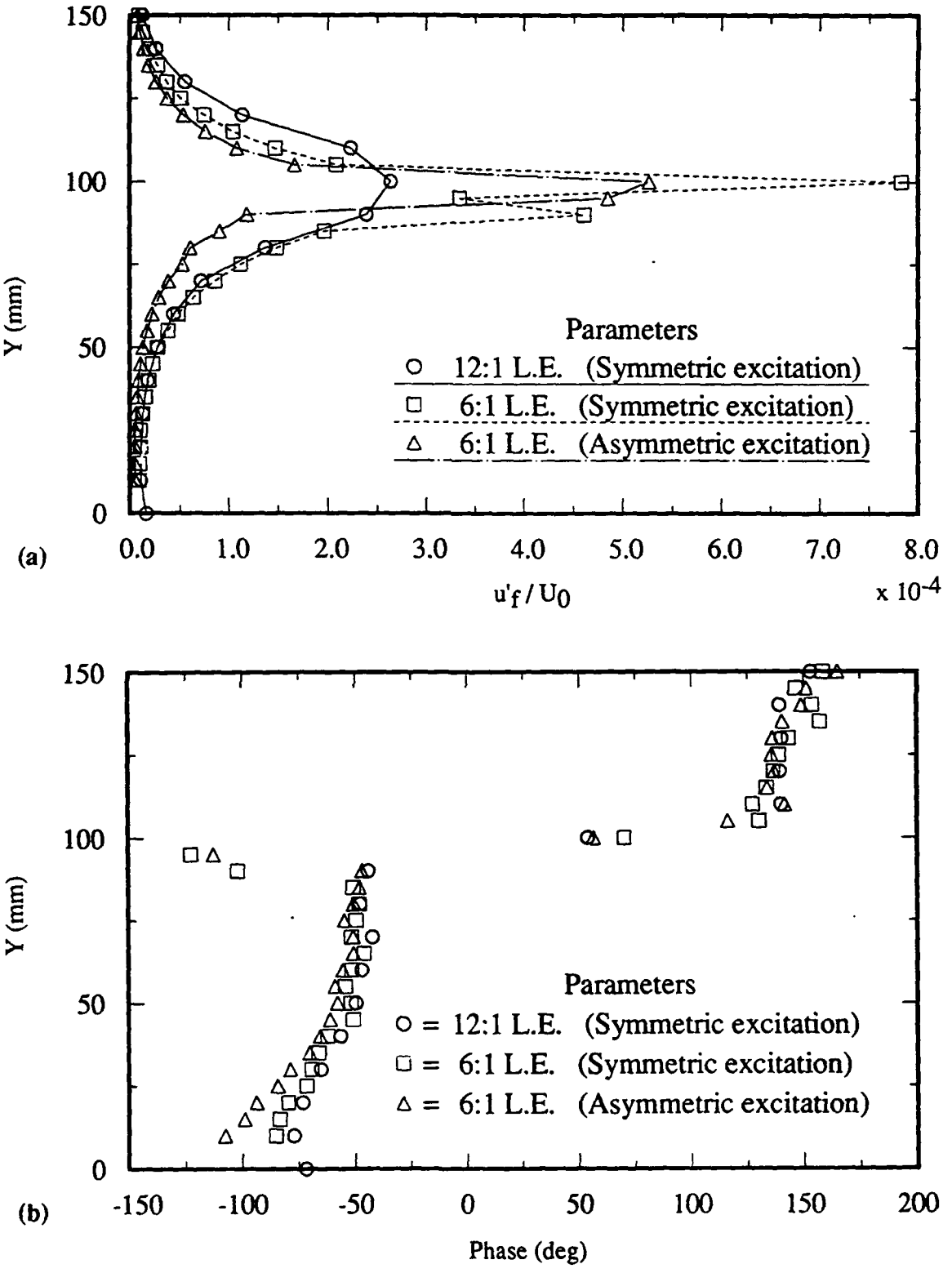

Figure 9. Single ribbon wake profiles of streamwise perturbation velocity (a) amplitude and (b) phase for Y_0 = 102 mm. Note that in this case the plate is installed.

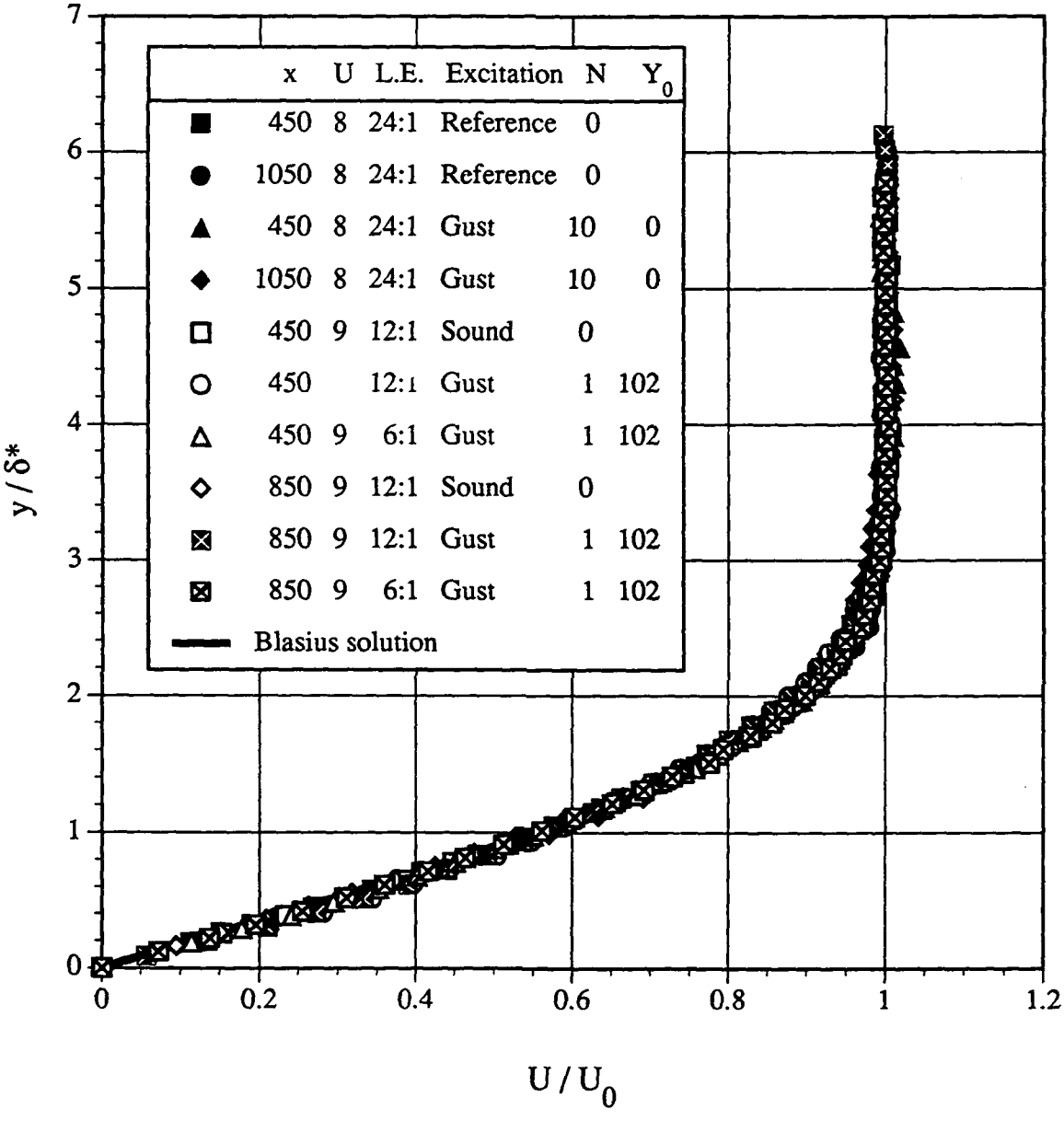

Figure 10. Comparison of mean boundary layer profiles for various configurations and excitation conditions.

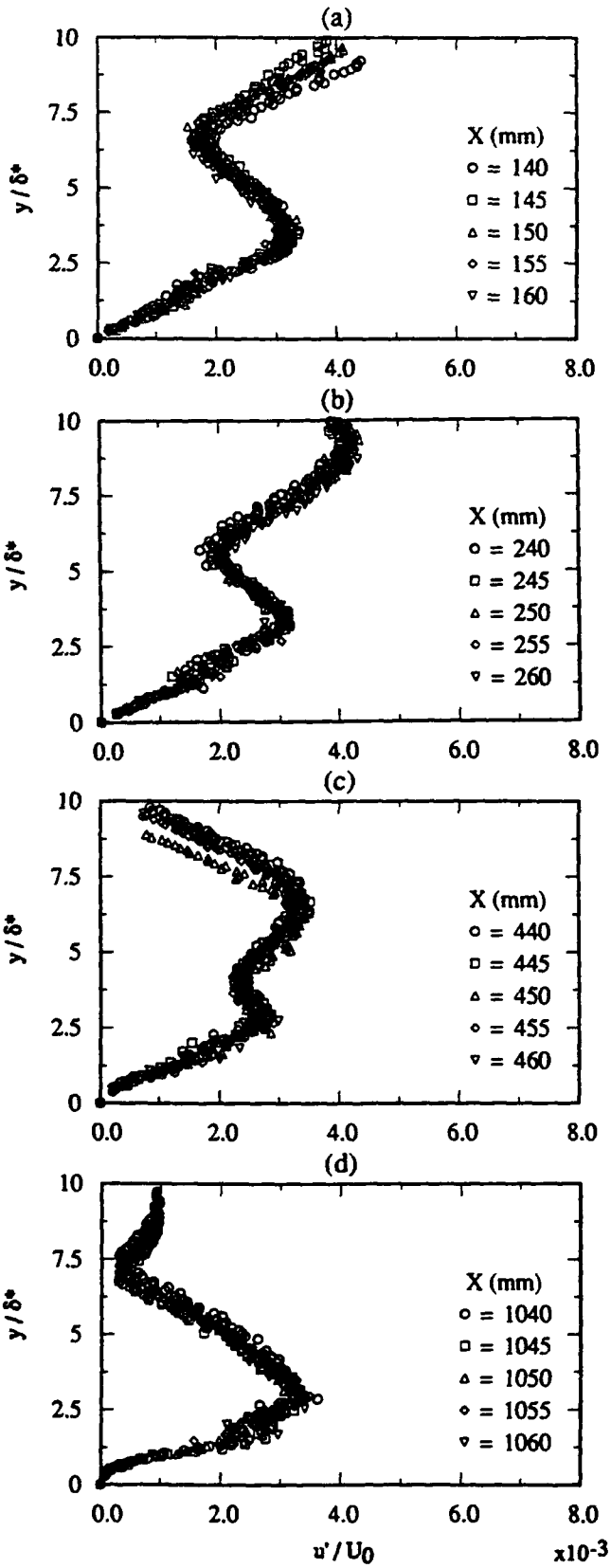

Fig. 11. Full u' profiles as a function of x; U_0=8m/s; 50-Hz convected gust excitation; F=81 x 10^{-6}; A=9.8 m/s^2.

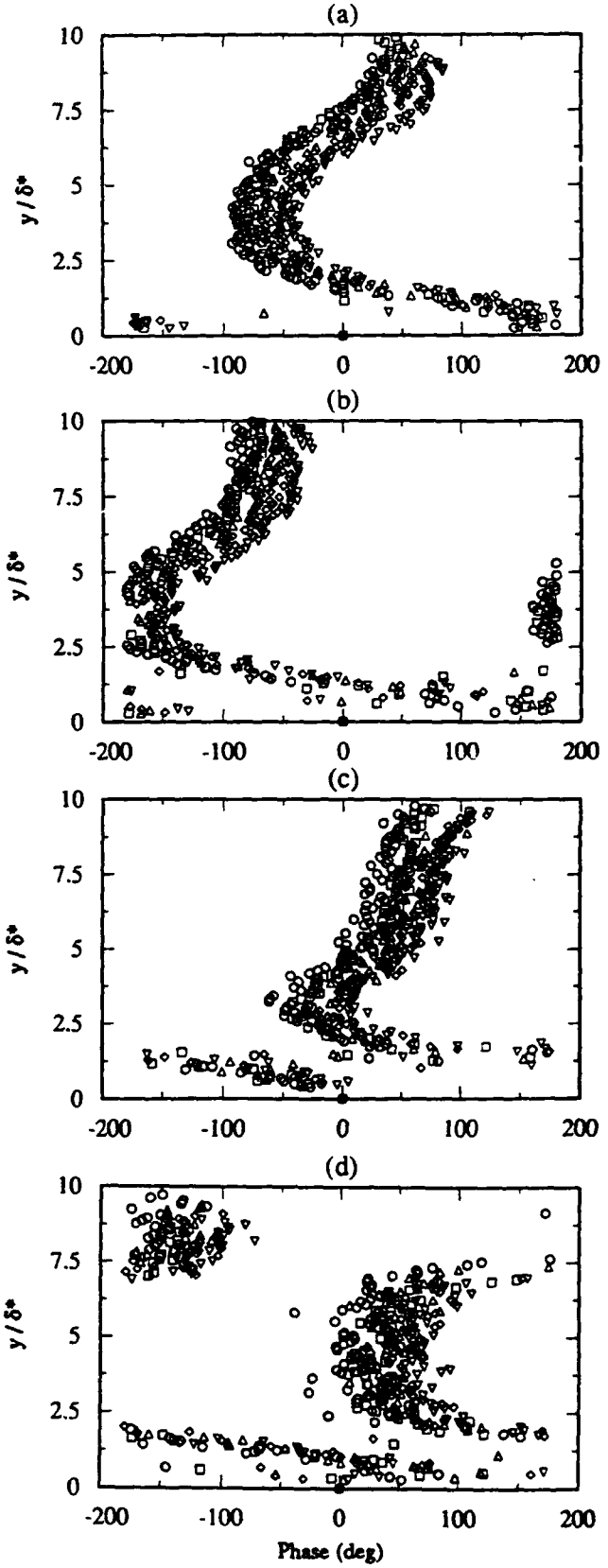

Fig. 12. Phase profiles as a function of x; U_0=8m/s; 50-Hz convected gust excitation; F=81 x 10^{-6}; A=9.8 m/s^2.

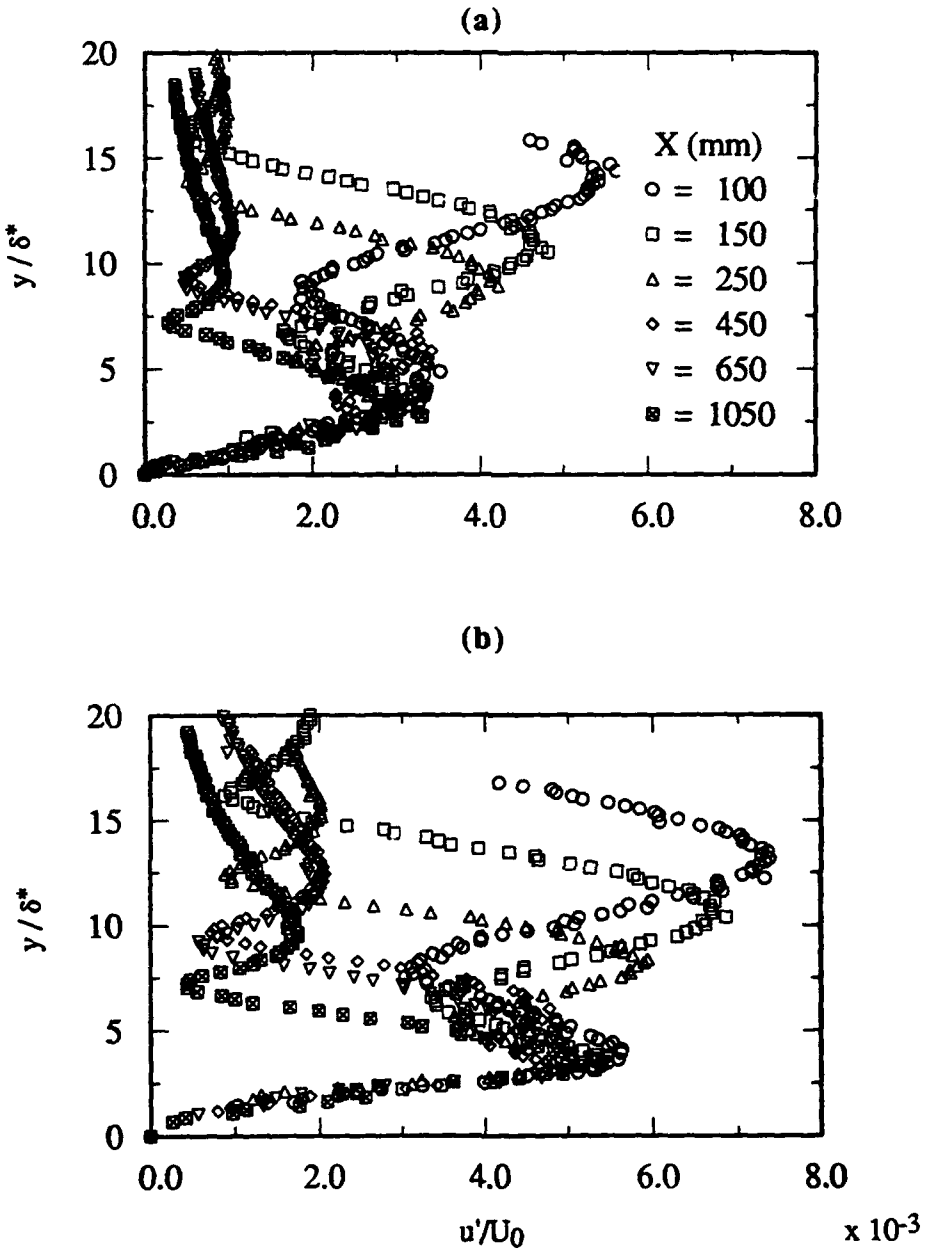

Fig. 13. Comparison of convected gust cases at different excitation frequencies; U_0=8 m/s; A=9.8 m/s^2; (a) f=50 Hz (F=81 x 10^{-6}) and (b) f=70 Hz (F=113 x 10^{-6}).

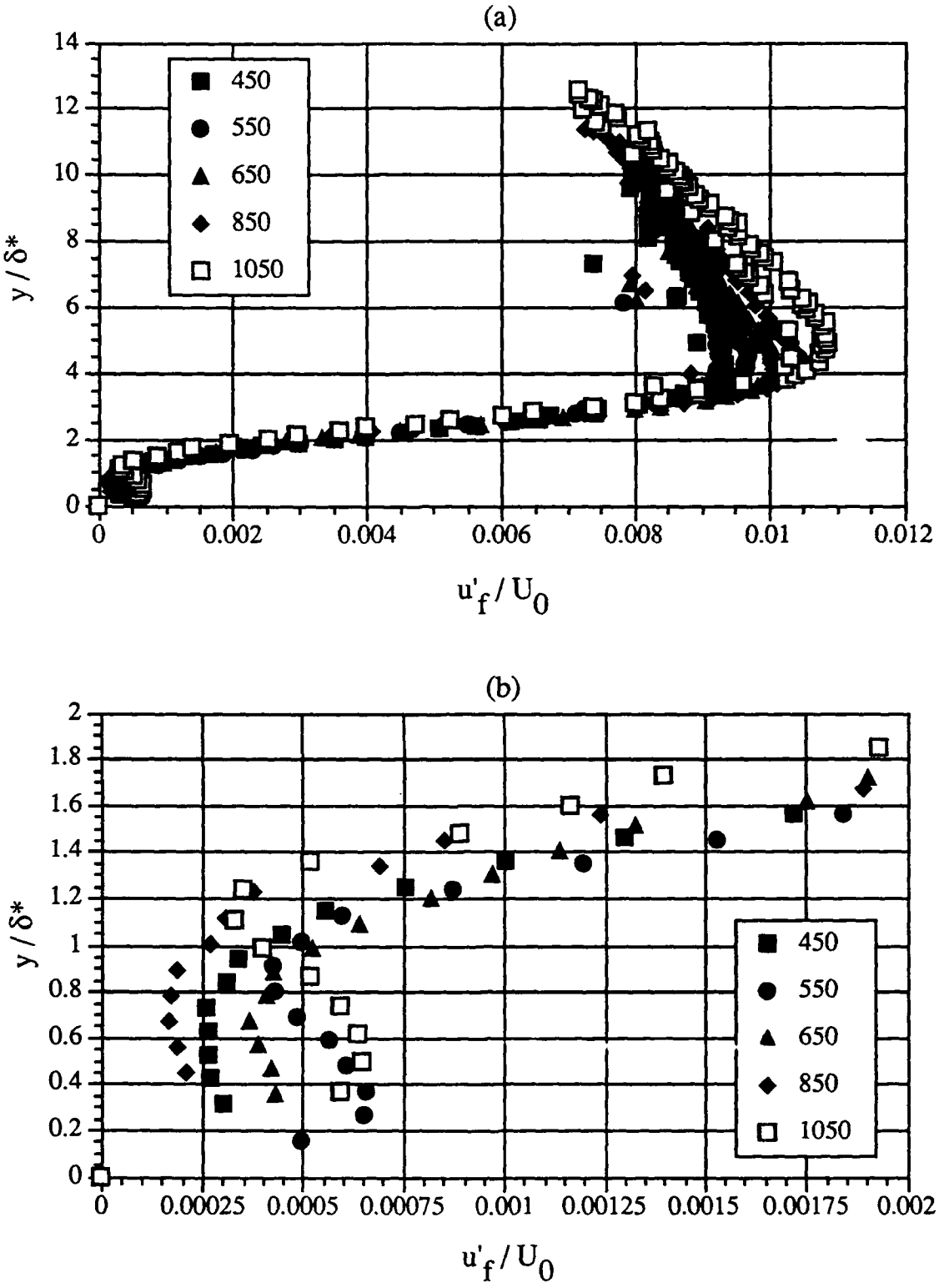

Figure 14. Streamwise perturbation velocity profiles as a function of x for external wake case (Y_0 = 64 mm); (a) full profile and (b) near-wall profile; f = 50 Hz (F = 81 x 10^{-6}); U_0 = 8 m/s; A = 34.3 m/s^2. Legends denote x-location in mm.

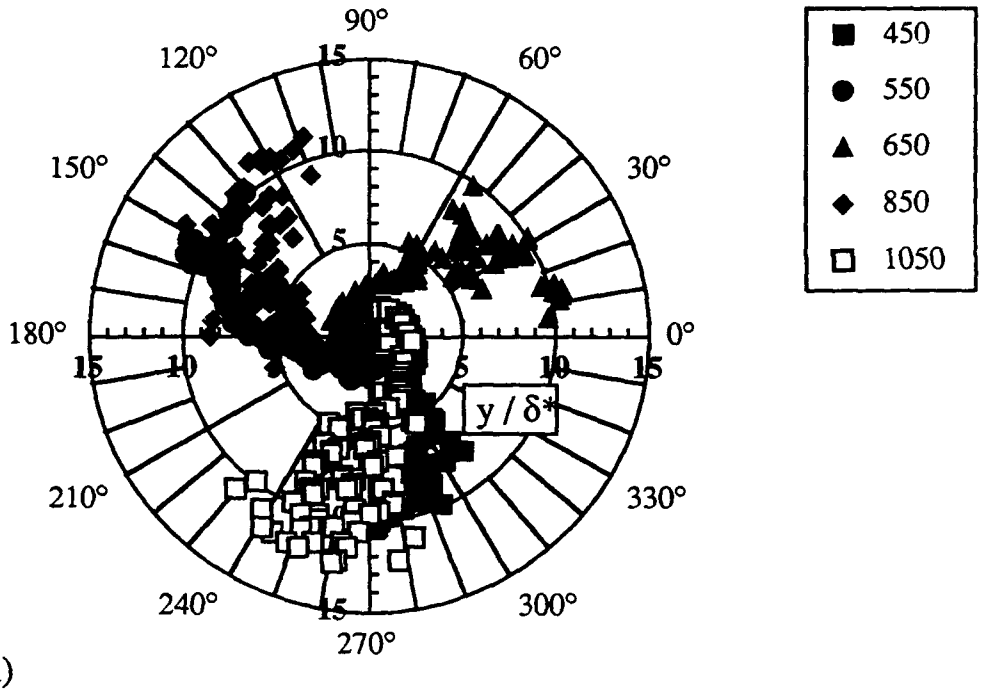

(a)

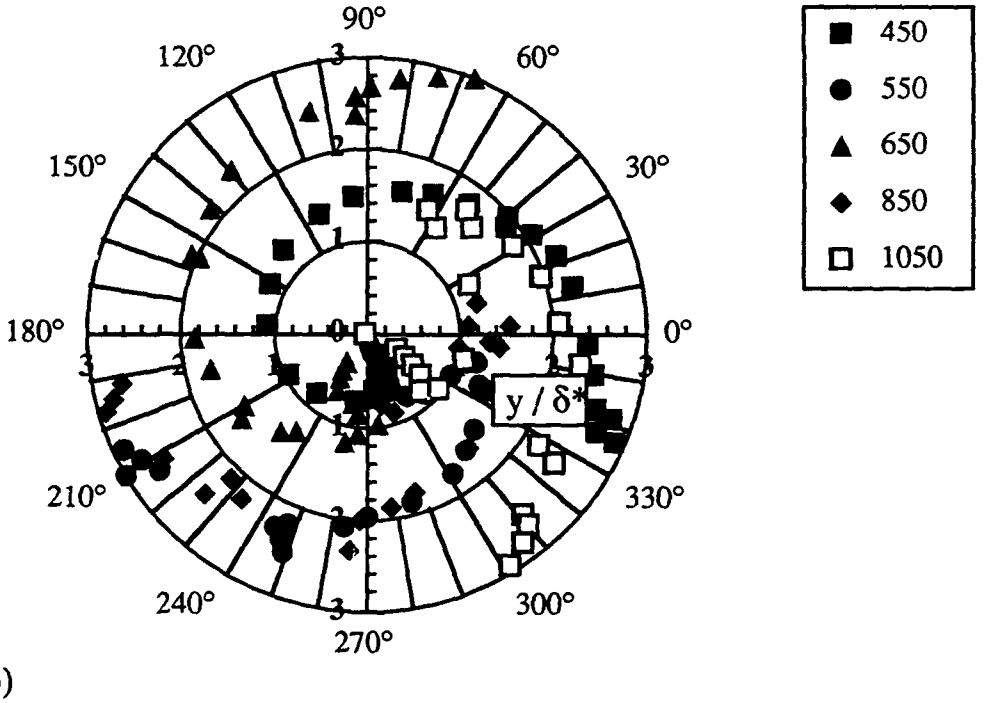

(b)

Figure 15. Phase profiles of perturbation velocity as a function of x for external wake case (Y_0 = 64 mm); (a) full profile and (b) near-wall profile; f = 50 Hz (F = 81 x 10^{-6}); U_0 = 8 m/s; A = 34.3 m/s^2. Legends denote x-location in mm.

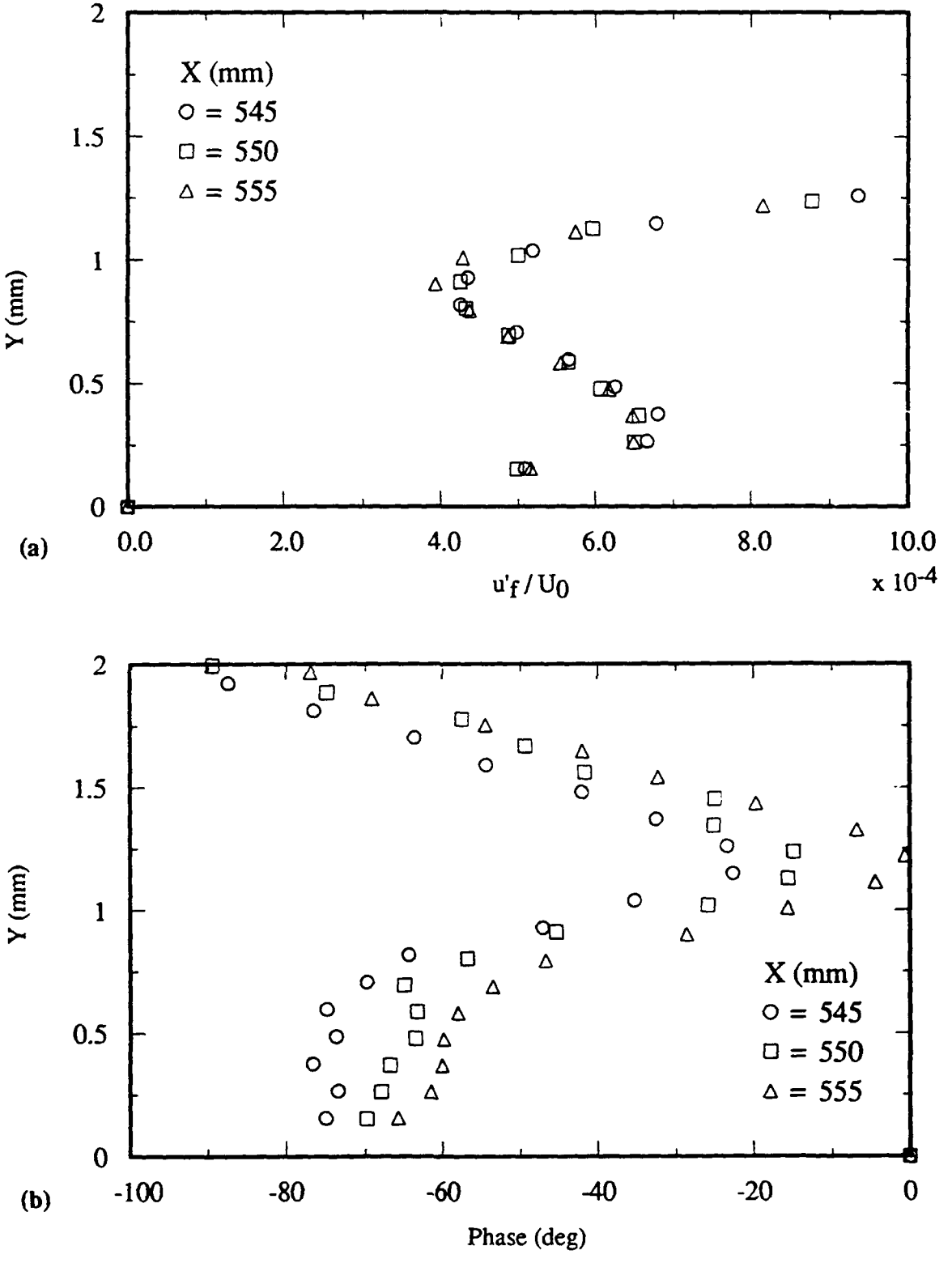

Figure 16. A closely spaced set of streamwise perturbation (a) amplitude and (b) phase profiles for external wake case. Same parameters as in Figs. 14 and 15.

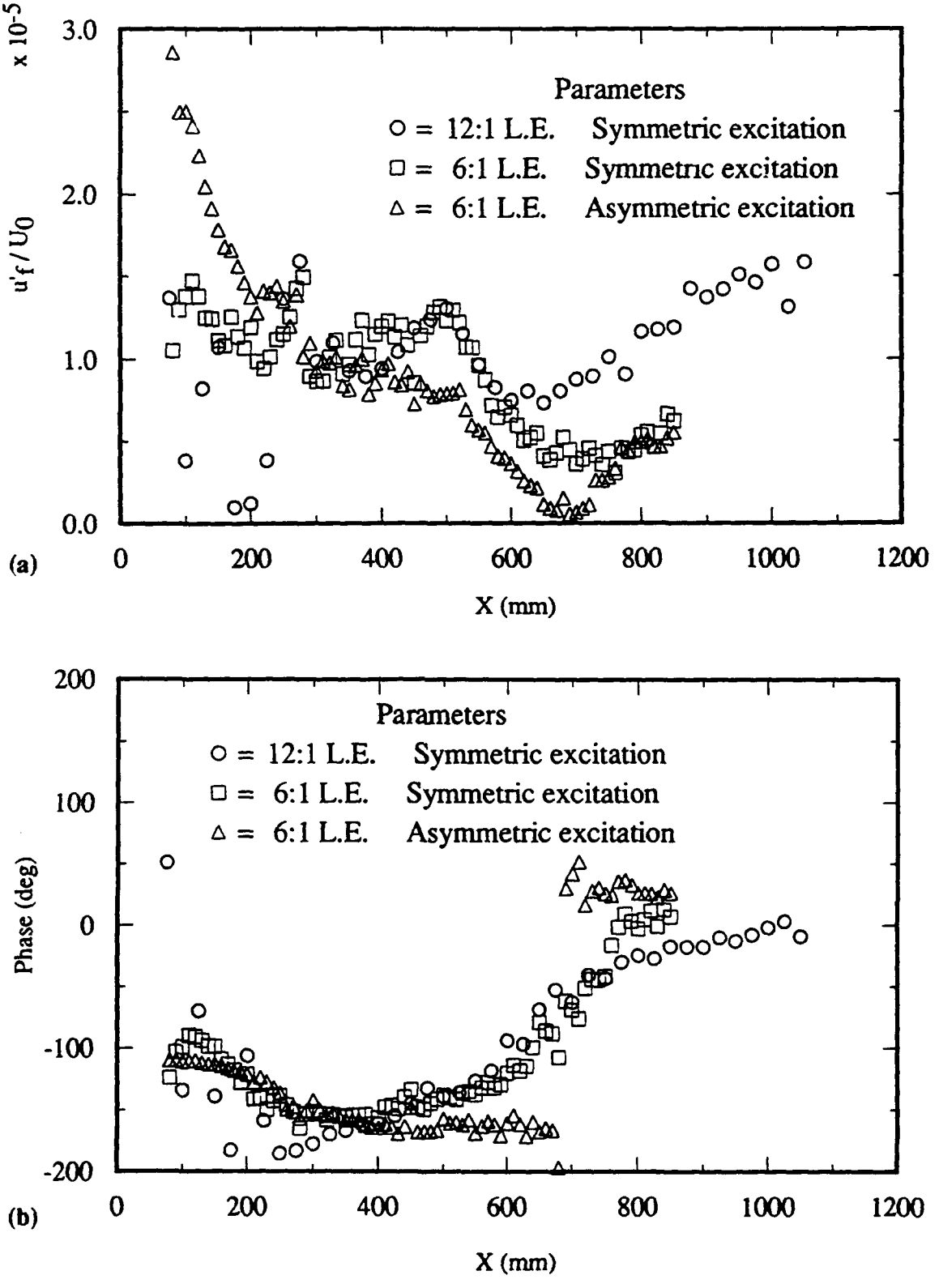

Figure 17. Streamwise evolution of perturbation (a) amplitude and (b) phase for single-ribbon excitation (Y_0 = 102 mm); U_0 = 9 m/s and f = 84.4 Hz.

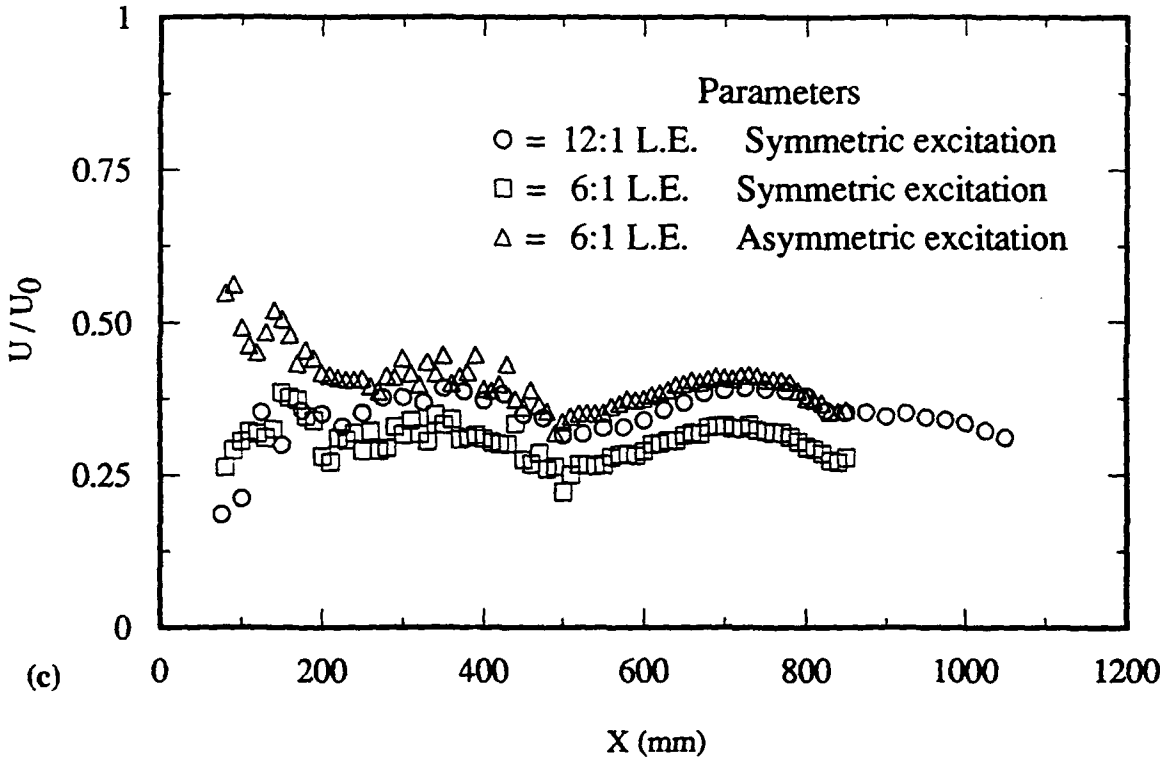

Figure 17c. Local mean velocity corresponding to data in (a) and (b).

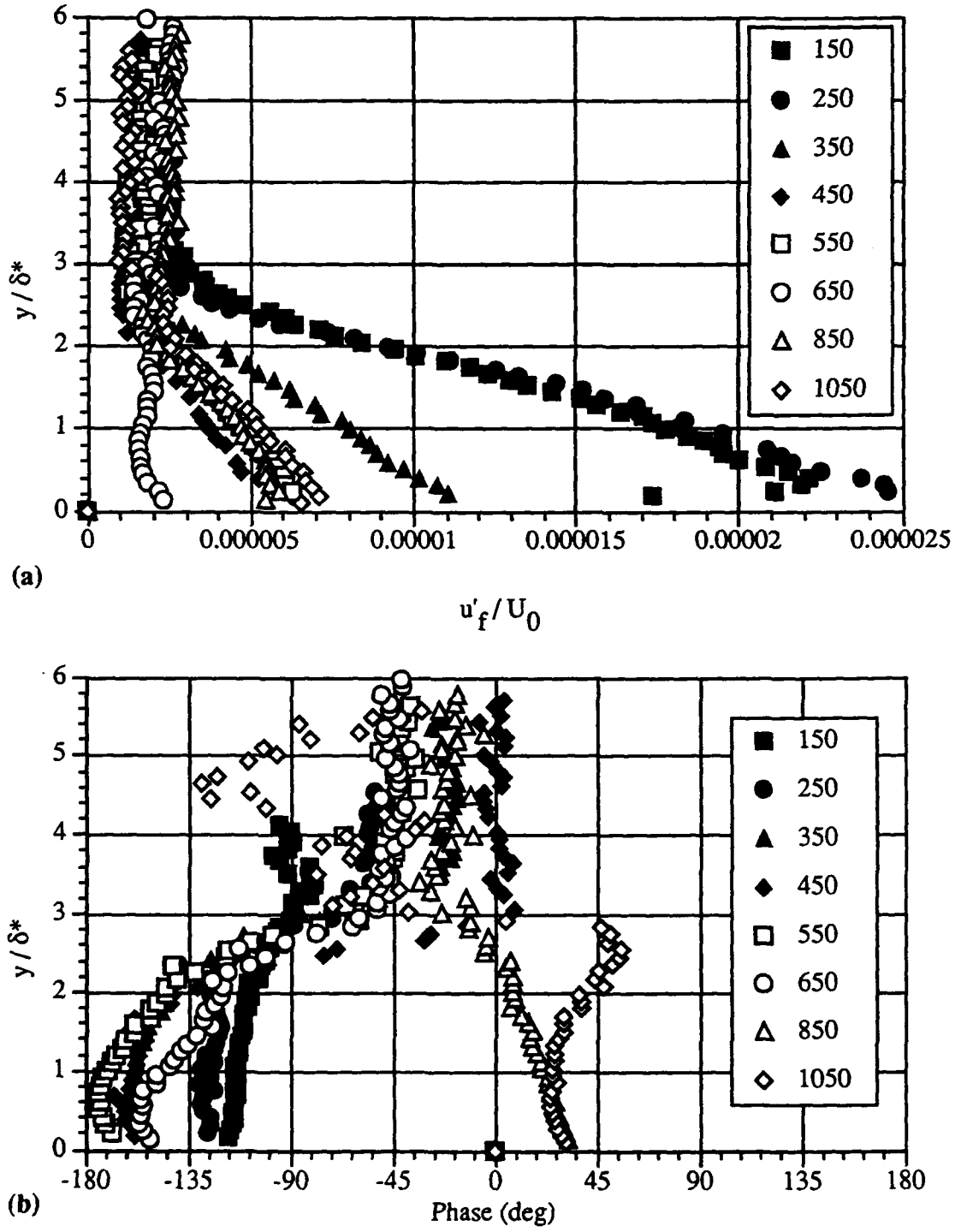

Figure 18. Streamwise velocity perturbation (a) amplitude and (b) phase for single-ribbon external wake (Y_0 = 102 mm) asymmetric excitation. Configuration includes 6:1 leading edge and rectangular bump. U = 9 m/s and f = 84.4 Hz.